



**New features in
WRF-SFIRE and the
system in Israel**

J. Mandel et al.

New features in WRF-SFIRE and the wildfire forecasting and danger system in Israel

**J. Mandel^{1,2}, S. Amram^{3,4}, J. D. Beezley⁵, G. Kelman^{3,6}, A. K. Kochanski⁷,
V. Y. Kondratenko¹, B. H. Lynn^{3,6}, B. Regev^{3,4}, and M. Vejmelka^{1,2}**

¹University of Colorado Denver, Denver, CO, USA

²Institute of Computer Science, Czech Academy of Sciences, Prague, Czech Republic

³The Hebrew University in Jerusalem, Jerusalem, Israel

⁴Ministry of Public Security, Jerusalem, Israel

⁵CERFACS and Météo France, Toulouse, France

⁶Weather It Is, LDT, Efrat, Israel

⁷University of Utah, Salt Lake City, UT, USA

Received: 20 December 2013 – Accepted: 17 January 2014 – Published: 24 February 2014

Correspondence to: J. Mandel (jan.mandel@gmail.com)

Published by Copernicus Publications on behalf of the European Geosciences Union.

Title Page

Abstract

Introduction

Conclusions

References

Tables

Figures



Back

Close

Full Screen / Esc

Printer-friendly Version

Interactive Discussion



Abstract

Recent advances in computational capabilities of computer clusters made operational deployments of coupled atmosphere-fire models feasible, as the weather and fire spread forecast can be nowadays generated faster than real time. This paper presents new developments in the coupled WRF-SFIRE model and related software in past two years, being a response to the needs of the community interested in operational testing of WRF-SFIRE. We describe a new concept of the fireline intensity intended to better inform about the local fire front properties and fire danger. We present a fuel moisture model and a fuel moisture data assimilation system based on the Remote Automated Weather Stations (RAWS) observations, allowing for fire simulations across landscapes and time scales of varying fuel moisture conditions. The paper also describes the implementation of a coupling with the atmospheric chemistry and aerosol schemes in WRF-Chem allowing for simulation of smoke dispersion and effects of fires on air quality, as well as a data assimilation method allowing for starting the fire simulations from an observed fire perimeters instead of ignition points. Finally, an example of an operational deployment and new visualization and the data management tools are presented.

1 Introduction

Wildland fire is a complicated multiscale process. The fire behavior is affected by very small-scale processes occurring at the flames (pyrolysis, combustion). Slightly larger-scale turbulent processes induce mixing of the combustible gasses with the ambient air, and transport of heat, moisture and combustion products into the atmosphere affecting the fire as well. In a case of a wildland fire, all these processes, no matter how small-scale, are affected to some degree by larger scale weather conditions since the energy from larger scales drives a cascade of gradually smaller and smaller eddies. Synoptic flows interact with topography and land use characteristics, and generate local winds

NHESSD

2, 1759–1797, 2014

New features in WRF-SFIRE and the system in Israel

J. Mandel et al.

Title Page

Abstract

Introduction

Conclusions

References

Tables

Figures

⏪

⏩

◀

▶

Back

Close

Full Screen / Esc

Printer-friendly Version

Interactive Discussion



New features in WRF-SFIRE and the system in Israel

J. Mandel et al.

Title Page

Abstract

Introduction

Conclusions

References

Tables

Figures

⏪

⏩

◀

▶

Back

Close

Full Screen / Esc

Printer-friendly Version

Interactive Discussion



that drive wildland fire propagation. Large-scale weather patterns induce changes in temperature and humidity that affect fuel moisture, thus affecting the fire behavior as well. If a fully physical representation of the wildland fire propagation were chosen, all this range of scales would have to be modeled. Although this approach is technically feasible to some degree for very small fires (Linn and Cunningham, 2005; Mell et al., 2007), the massive computational costs of such simulations make them prohibitive from the operational point of view. Also, capturing within one model the small-scale combustion processes and large scale weather conditions including clouds, winds and precipitation is practically impossible. Fortunately, coupling of a mesoscale weather model with a simple 2-D fire spread model allows to capture a practically important range of wildland fire behavior.

Wildland fires are closely coupled with the atmosphere. Winds drive the fire propagation. Conversely, the fire influences the weather through the heat and vapor fluxes from burning hydrocarbons and evaporation. The buoyancy created by the heat from the fire can cause intense updrafts inducing very strong surface winds, which in turn affect the fire. The fire-induced updrafts may also generate pyro-cumulus and fire storms. Therefore, a large fire may significantly affect the local atmospheric conditions, creating “its own weather.” The atmosphere interacts also with the fuel properties. Periods of warm and hot weather decrease fuel moisture increasing the fire hazard, and making fires more intense. Conversely, local precipitations or nocturnal moisture recovery tend to decrease fuel combustibility and inhibit fire spread. Coupling a weather model with a simple fire spread model and a simple fuel moisture model allows to capture these interactions, without explicit resolving of the small scale combustion and water adsorption processes, in a computationally modest way.

WRF-SFIRE (Mandel et al., 2009, 2011a) combines the Weather Research and Forecasting Model (WRF) (Skamarock et al., 2008), with the fire spread (SFIRE) implemented by the level-set method. WRF-SFIRE is a two-way coupled fire-atmosphere model, so the heat fluxes from fire component provide forcing to the atmosphere, which influences winds, which in turn modify the fire spread. Similar models include MesoNH-

**New features in
WRF-SFIRE and the
system in Israel**J. Mandel et al.

Title Page

Abstract

Introduction

Conclusions

References

Tables

Figures

◀

▶

◀

▶

Back

Close

Full Screen / Esc

Printer-friendly Version

Interactive Discussion



ForeFire (Filippi et al., 2011). Recently, the model was expanded with fuel moisture model, and chemical transport of emissions (Fig. 1). The model is able to run faster than real time on several hundred cores, with the fire model resolution of few meters and horizontal atmospheric resolution on the order of 100 m, for a large real fire (Jordanov et al., 2012). However, the operational deployment discussed in Sect. 8 uses coarser meshes on a smaller number of processors.

WRF-SFIRE has evolved from CAWFE (Clark et al., 2004; Coen, 2005). The code currently supports the semi-empirical fire spread model (Rothermel, 1972), inherited from the CAWFE code. Support of alternative fire spread models (Balbi et al., 2009; Fendell and Wolff, 2001) is in progress. The current code and documentation are available from OpenWFM.org. A version from 2010 is distributed with the WRF release as WRF-Fire (Coen et al., 2012; OpenWFM, 2012).

Validation studies of WRF-SFIRE are now available for a large-scale wildfire (Kochanski et al., 2013c) as well as for a microscale simulation of a grass burn experiment (Kochanski et al., 2013d). The coupling of the fire heat release with the atmosphere allows a detailed study of the effect of wind shear on fire propagation (Kochanski et al., 2013a). Examples of work from other groups using WRF-SFIRE include Simpson et al. (2013) and Peace et al. (2011).

This paper consolidates for the first time in a journal form new developments in the SFIRE software system in the two years since the reference paper Mandel et al. (2011a), scattered in presentations and conference abstracts, and complements them by new results. New fireline intensity and fire danger assessment tools are described in Sect. 2, ignition in the coupled atmosphere-fire model from a developed fire perimeter in Sect. 3, fuel moisture model and a real test case in Sect. 4, and assimilation of RAWS fuel moisture data in Sect. 5. New software developments include interfaces to GIS (Sect. 6), coupling with smoke transport and atmospheric chemistry by WRF-Chem (Sect. 7), and an operational deployment (Sect. 8). We do not describe the basic principles, operation, and history of the core of WRF-SFIRE here, and refer to Mandel et al. (2011a) and the User's Guide (OpenWFM, 2013) instead.

2 New fireline intensity and fire danger mapping

Our users requested maps that would help them assess the fire risk at any particular location. Such estimates answer the question, “how bad would be a fire here?”. Such assessments help the authorities with declaring fire-bans and with allocation of fire-fighting and fire prevention resources. Therefore, variables characterizing a potential fire are of interest and they can be used to plot potential fire severity maps. This is a concept similar to FLAMMAP, which computes various potential fire characteristics (Finney, 2006).

One such obvious quantity is the fire spread rate, which is already produced by SFIRE, but only at the fireline, because the fire spread rate depends on the direction of fire propagation. Therefore, a diagnostic variable was added, equal to the maximal rate of spread at any location, given the wind speed and the slope. The spread rate of a potential fire, however, does not capture the actual heat output of the fire, which can be very different for different fuels even with the same spread rate. Byram’s fireline intensity (Byram, 1959) is the heat produced per unit length of the fireline in unit time ($\text{Jm}^{-1} \text{s}^{-1}$) in the so-called flaming zone behind the fireline.

Byram’s fireline intensity is given by

$$I = HRw, \quad (1)$$

where H (Jkg^{-1}) is the heat content of the fuel, R (ms^{-1}) is the spread rate, and w (kgm^{-2}) is the fuel amount that burns in the flaming zone. In practice, the fuel amount burned w is estimated as a fixed fraction of the fuel load w_0 (kgm^{-2}), typically 0.9. Byram’s fireline intensity is routinely used for practical guidance and it has been linked statistically to flame length for the purpose of assessing the difficulty approaching the fireline. However, its weakness is that it does not depend on the combustion rate. Generally, if the combustion rate is low (the fuel burn slowly), much of the burning takes place at a distance from the fire front. In this case, the advancing fire front leaves burning fuel behind it, which does not contribute much to the fireline properties itself. On the

NHESSD

2, 1759–1797, 2014

New features in WRF-SFIRE and the system in Israel

J. Mandel et al.

Title Page

Abstract

Introduction

Conclusions

References

Tables

Figures

◀

▶

◀

▶

Back

Close

Full Screen / Esc

Printer-friendly Version

Interactive Discussion



contrary, fuel of a high combustion rate (burning fast), releases heat quickly and very close to the fire line. In this case practically no burning fuel is left behind the fire front so most of the combustions heat contributes to the fire intensity at the fire front.

Therefore, a new concept of fireline intensity was introduced (Mandel et al., 2011b) as the amount J of heat generated by the advancing fireline from the newly burning fuel only, in a small unit of time. Assume that the fuel fraction after ignition decreases exponentially with the time t from ignition, as e^{-t/T_f} , where T_f is the fuel burn time, i.e., the time when $1 - e^{-1} \approx 63\%$ of fuel has burned. Then,

$$J = \frac{HRw_0}{2T_f} \text{ (Jm}^{-1}\text{s}^{-2}\text{)}. \quad (2)$$

Unlike Byram's fireline intensity (Eq. 1), the new fireline intensity, given by Eq. (2), takes into account the effect that a faster burning fuel will create a more intense heat concentrated at the fireline. The reason why the time unit is squared is that over a longer time, the fireline advances a longer distance, and the newly burning fuel will also burn longer.

To estimate the simulated fire severity, the code computes the fireline intensities and the reaction intensity (which is the same as the released heat flux intensity, $\text{Js}^{-1}\text{m}^{-2}$). The fireline intensities are computed from the fire rate of spread R . Since R is well-defined on the fireline only, the fireline intensities are defined on mesh nodes next to the fireline only as well. Separate computations are made as a component of a fire danger rating to estimate the severity of a potential fire, using the maximum spread rate in any direction.

3 Initialization from a fire perimeter

A fire model starts a fire simulation from a known ignition point at a known ignition time. However, users are interested in starting the model from an existing fire, whose

New features in WRF-SFIRE and the system in Israel

J. Mandel et al.

Title Page

Abstract

Introduction

Conclusions

References

Tables

Figures

◀

▶

◀

▶

Back

Close

Full Screen / Esc

Printer-friendly Version

Interactive Discussion



presence has just been detected and mapped. The ignition point and ignition time typically become known too late to be relevant for real-time simulation and forecasting.

Thus, we are interested in starting a fire simulation from a given fire perimeter at a given time, from now on, called the *perimeter time*. However, the fuel balance and the state of the atmosphere depend on the history of the fire, which is not known. We propose to create an approximate artificial history of the fire based on the given fire perimeter and the perimeter time, the fuel map, and the state of the atmosphere during the period before the perimeter time. The history is encoded as the time of ignition, given at every node in the domain, also known in the literature as the fire arrival time. We then run the fire-atmosphere model as usual, except we use the prescribed ignition time instead of the spread model until the perimeter time. By replaying the artificial fire history, we burn the fuel and release the heat into the atmosphere gradually, and hopefully allow a proper fuel balance and an atmospheric circulation to develop, corresponding to the given fire perimeter. At the perimeter time, the complete coupled atmosphere-fire model takes over.

In Kondratenko et al. (2011), we have used ignition times in the fire area, calculated based on the distance from a known ignition point to the perimeter, while use of the reinitialization equation was proposed in Mandel et al. (2012). Our current approach consists of reversing the direction of time in a fire spread method, thus shrinking the fire to one or more ignition points. We have first developed a new fire spread method, which determines the ignition time at a node as the earliest time the fire can get to that node from the nodes that are already burning (Fig. 2a). Such methods are known as minimal travel or minimal fire arrival time (Finney, 2002). A list of nodes on the boundary of the already burning region is maintained similarly as in the fast marching method (Sethian, 1999). The additional complication here is that the fire travel time from one node to the next changes dynamically, because it depends on the wind at the moment through the spread rate. To build the artificial fire history, we reverse the direction of the time, start from nodes nearest to the perimeter, and proceed inside the domain. The ignition time propagates to nodes that were not already processed as the

NHESSD

2, 1759–1797, 2014

New features in WRF-SFIRE and the system in Israel

J. Mandel et al.

Title Page

Abstract

Introduction

Conclusions

References

Tables

Figures

⏪

⏩

◀

▶

Back

Close

Full Screen / Esc

Printer-friendly Version

Interactive Discussion



maximum ignition time given the ignition times already known, instead of the minimum arrival time (Fig. 2b).

Simulation results for an ideal example show that the fire can continue in a natural way from the perimeter ignition (Kondratenko et al., 2011). Here we demonstrate perimeter ignition on the simulation of the 2007 Santa Ana fires from Kochanski et al. (2013c). These are two fires, Witch and then Guejito, which merged quickly into one massive fire. The perimeter from the simulation at 20:00:00 22 October 2007 UTC is in Fig. 3a, and the artificial ignition time created is shown in Fig. 3b. The artificial ignition graph has two minima, which correspond to the two ignition points and times. Figure 4 shows a comparison of the wind from the original simulation and with the artificial ignition times. We have then continued the simulation for additional 6 h to assess the effect of the perimeter ignition on further propagation of the fire (Fig. 5). Again, the original simulation, which plays the role of the truth here, and the simulation started from the perimeter ignition, are quite close.

4 Fuel moisture model

Fire spread rate depends strongly on the moisture contents of the fuel, therefore modeling fuel moisture is important. Fuel responds to atmospheric conditions by evaporating or absorption of moisture from the air, as well as soaking moisture when it rains. The following simple approach (Kochanski et al., 2012; Mandel et al., 2012) models the evolution of fuel moisture response by a first order differential equation, running at each node of the surface mesh independently.

Following the model from Van Wagner and Pickett (1985, Eqs. 4 and 5), over a long time in constant temperature T (K) and relative humidity H (%), the water contents m in dead wood will approach the drying equilibrium

$$E_d = 0.924H^{0.679} + 0.000499e^{0.1H} + 0.18(21.1 + 273.15 - T)(1 - e^{-0.115H})$$

New features in WRF-SFIRE and the system in Israel

J. Mandel et al.

Title Page

Abstract

Introduction

Conclusions

References

Tables

Figures

◀

▶

◀

▶

Back

Close

Full Screen / Esc

Printer-friendly Version

Interactive Discussion



when starting from $m > E_d$, and the wetting equilibrium

$$E_w = 0.618H^{0.753} + 0.000454e^{0.1H} + 0.18(21.1 + 273.15 - T)(1 - e^{-0.115H})$$

when starting from $m < E_w$. The evolution of the fuel moisture in time is then modeled by the time-lag differential equation with characteristic lag time T_L ,

$$\frac{dm}{dt} = \begin{cases} \frac{E_d - m}{T_L} & \text{if } m > E_d \\ 0 & \text{if } E_d \geq m \geq E_w \\ \frac{E_w - m}{T_L} & \text{if } m < E_w \end{cases} \quad (3)$$

During rain, the equilibrium moisture E_d or E_w is replaced by the saturation moisture contents S , and Eq. (3) is modified to achieve the rain-wetting lag time T_r for heavy rain only asymptotically, when the rain intensity r (mm h^{-1}) is large:

$$\frac{dm}{dt} = \frac{S - m}{T_r} \left(1 - \exp\left(-\frac{r - r_0}{r_s}\right) \right), \text{ if } r > r_0, \quad (4)$$

where r_0 is the threshold rain intensity below which no perceptible wetting occurs, and r_s is the saturation rain intensity. At the saturation rain intensity, $1 - 1/e \approx 63\%$ of the maximal rain-wetting rate is achieved. We have calibrated the coefficients to achieve a similar behavior as the rain-wetting model in the Canadian fire danger rating system (Van Wagner and Pickett, 1985), which estimates the fuel moisture as a function of the initial moisture contents and rain accumulation over 24 h. For 10 h fuel, we have obtained the coefficients $S = 250\%$, $T_r = 14$ h, $r_0 = 0.05 \text{ mm h}^{-1}$ and $r_s = 8 \text{ mm h}^{-1}$, cf., Fig. 6.

The model maintains the fuel moisture contents m_k at the center of each atmospheric grid cell on the surface for several fuel classes k , such as 1 h, 10 h, 100 h, and 1000 h fuel. Because the atmospheric mesh is relatively coarse, this is quite cheap, and we also avoid any difficulties with nonhomogeneous fuel distribution, because the

New features in WRF-SFIRE and the system in Israel

J. Mandel et al.

Title Page

Abstract

Introduction

Conclusions

References

Tables

Figures

◀

▶

◀

▶

Back

Close

Full Screen / Esc

Printer-friendly Version

Interactive Discussion



model is independent of the fuel map. The actual fuel is assumed to be a mixture of those classes in known proportions $w_k \geq 0$ given by the fuel category. The fuel moisture contents in each cell on the (finer) fire mesh with is then obtained by interpolating the moisture content m_k to the finer grid for each fuel class, and then computing the weighted average $\sum_{k=1}^N w_k m_k$.

Because the model needs to support an arbitrarily long time step, we have chosen an adaptive exponential method to integrate the fuel moisture equations at every grid node. Equations (3) and (4) have the common form

$$\frac{dm}{dt} = \frac{E - m}{T}. \quad (5)$$

On the time interval $[t_n, t_{n+1}]$, we first approximate the coefficient E and T by constants $E_{n+1/2}$ and $T_{n+1/2}$ by averaging the atmospheric state variables at t_n and t_{n+1} , and then solve the resulting constant coefficient equation exactly over the time step interval $[t_n, t_{n+1}]$,

$$M_{n+1} = M_n + (E_{n+1/2} - M_n) \left(1 - e^{-\Delta t/T_{n+1/2}}\right), \Delta t = t_{n+1} - t_n. \quad (6)$$

For short time steps, $\Delta t/T_{n+1/2} < \varepsilon = 0.01$, the exponential in Eq. (6) is replaced by the Taylor expansion $1 - e^{-x} \approx x$ to avoid a large relative rounding error caused by subtracting two almost equal quantities. The resulting method is exact for arbitrarily large Δt when the coefficients are constant in time, and it is of second order as $\Delta t \rightarrow 0$.

The fuel moisture model has been tested on the simulation of the Barker Canyon Complex fire, which started on 8 September 2012, around 8 p.m. PDT, 10 miles NW from the Grand Coulee Dam in Washington. The 108 h-long simulations were performed using a set of 5 nested domains of gradually increasing resolutions: 36 km, 12 km, 4 km, 1.33 km, and 444 m, with time steps 162 s, 54 s, 18 s, 6 s, and 2 s, respectively (Fig. 7a). The Mellor–Yamada–Janjic PBL scheme and the Kain–Fritsch cumulus scheme were used on the three coarsest domains. In order to fully utilize LANDFIRE

**New features in
WRF-SFIRE and the
system in Israel**

J. Mandel et al.

Title Page

Abstract

Introduction

Conclusions

References

Tables

Figures

◀

▶

◀

▶

Back

Close

Full Screen / Esc

Printer-friendly Version

Interactive Discussion



Discussion Paper | Discussion Paper | Discussion Paper | Discussion Paper | Discussion Paper

fuel, and elevation data provided at 30 m resolution, the innermost fire domain had a further refined fire mesh of 22.2 m (1 : 20 refinement ratio). The atmospheric component of the model was initialized and forced at the boundaries by the Northern American Regional Reanalysis (NARR) providing meteorological data at 3 h intervals.

5 There were no ground fuel moisture observations available within the fire domain, so the 1 h fuel moisture was initialized with its equilibrium value, while the initial 10 h, 100 h and 1000 h fuel moistures were approximated using data from the National Fuel Moisture Database (4.0 %, 8.0 %, 7.0 % respectively). The southern branch of the fire was started from the ignition point reported by the Incident Information System (<http://inciweb.nwcg.gov>). The northern branch was ignited using locations of four lightning strikes observed within the fire perimeter on the ignition day. The approximate locations of the fire ignition points are presented in Fig. 7b.

In order to assess the impact of the fuel moisture model on the modeled fire spread we performed three fire simulations. The first one took advantage of the fuel moisture model computing the fuel moisture changes in all fuel classes based on the local meteorological conditions simulated by the atmospheric component of the system. The other two simulations were performed with the temporally and spatially constant fuel moisture. In the first case, the fuel moisture was set to the 4 day average of fuel moisture simulated using the fuel moisture model (11.6%). In the second case, the fuel moisture was set to the initial value at the very beginning of the simulation (6.38%). The time series of the fire area simulated with the fuel moisture model and without it using the averaged constant fuel moisture are presented in Fig. 8. The fire spread clearly responds to the changes in the fuel moisture. The nighttime peaks in the fuel moisture are associated with the fire stagnation, while the daytime fuel drying promotes the rapid fire spread. The simulation with the fuel moisture model not only renders the diurnal variations in the fire activity but also improves the total simulated fire area. The simulation with the constant fuel moisture set to 11.6 % underestimated the fire area by a factor of three. On the other hand, the simulation performed with the constant fuel moisture initialized with a value corresponding to the initial value in the run with mois-

New features in WRF-SFIRE and the system in Israel

J. Mandel et al.

Title Page

Abstract

Introduction

Conclusions

References

Tables

Figures

⏪

⏩

◀

▶

Back

Close

Full Screen / Esc

Printer-friendly Version

Interactive Discussion



ture model (6.38 %), overestimated the fire area by a factor of 2. The run with the fuel moisture model provided a great improvement over the simulations with constant fuel moisture, and added diurnal variations in the fire activity not present in the run without it. The comparison between the spatial patterns of the Barker Canyon Complex fire simulated with and without the fuel model, as well as the fire perimeter detected on 13 September 2012 07:44 UTC, are presented in Fig. 7b. The fire extent simulated using the constant fuel moistures (white and red contours) do not compare well with the observations (green contour). The implementation of the time- and spatially-varying fuel moisture significantly improved the simulated fire perimeters of both the northern and the southern branches of the Barker Canyon Complex fire, see the blue contours in Fig. 7b.

5 Assimilation of RAWS fuel moisture data

To improve the quality of fuel moisture simulation, we have developed assimilation of fuel moisture measurements from station measurements. The Remote Automatic Weather Stations (RAWS) in the US also include measurements of fuel moisture. They measure the weight a sample of 10 h fuel exposed to the elements, and the resulting fuel moisture data are exported to <http://mesowest.utah.edu> continuously. The RAWS data are available hourly, but only at a small number of locations, which generally do not even coincide with grid nodes of our simulation grids.

We follow (Vejmelka et al., 2013) with some simplifications. To assimilate the moisture measurement into the differential Eq. (3) for each fuel class at each grid point, we augment the model state $(m_k)_{k=1,\dots,N_k}$ by perturbations ΔE and ΔS of the equilibrium moisture values: we replace E_d , E_w , and S in Eq. (3), by $E_d + \Delta E$, $E_w + \Delta E$, and $S + \Delta S$, respectively, and add the differential equations $d\Delta E/dt = 0$, $d\Delta S/dt = 0$. We then apply the standard extended Kalman filter to the model in the augmented variables

$$\mathbf{m}(t_i) = (m_1(t_i), m_2(t_i), \dots, m_{N_k}(t_i), \Delta E(t_i), \Delta S(t_i)).$$

**New features in
WRF-SFIRE and the
system in Israel**

J. Mandel et al.

Title Page

Abstract

Introduction

Conclusions

References

Tables

Figures



Back

Close

Full Screen / Esc

Printer-friendly Version

Interactive Discussion



Note that the common state variables ΔE and ΔS now couple the evolution of the different time-lag fuel moisture classes together.

We extend the measurements and their uncertainty from several RAWS locations to the whole domain using a trend surface model (Schabenberger and Gotway, 2005, § 5.3.1). We are looking for fuel moisture estimate $Z(s)$ at a location s in the form

$$Z(s) = \mathbf{X}_1(s)\boldsymbol{\beta}_1 + \dots + \mathbf{X}_k(s)\boldsymbol{\beta}_k + e(s), \quad (7)$$

where the fields \mathbf{X}_j are given fields, called covariates, and the errors $e(s) \sim N(0, \hat{\sigma}^2)$ independent, with $\hat{\sigma}^2$ the variance of the so-called microscale variability (the structure of the spatial field too small to be captured by the mesh). Given the measurements $\hat{Z}(s_i)$, $i = 1, \dots, n$, the coefficients $\boldsymbol{\beta}_j$ are found from the regression

$$\hat{Z}(s_i) = \mathbf{X}_1(s_i)\boldsymbol{\beta}_1 + \dots + \mathbf{X}_k(s_i)\boldsymbol{\beta}_k + \varepsilon(s_i) + e(s_i), i = 1, \dots, n, \quad (8)$$

where the errors $\varepsilon(s_i) \sim N(0, \gamma^2)$ are assumed to be independent, and also independent of $e(s_i)$. The variance γ^2 models the measurement error at the measurement station locations s_1, \dots, s_n . See Vejmelka et al. (2013) for a generalization when γ^2 is allowed to be different at different s_j .

The solution of the regression problem (Eq. 8) is obtained as the least-squares solution

$$\boldsymbol{\beta} = (\mathbf{X}(\mathbf{s})^T \mathbf{X}(\mathbf{s}))^{-1} \mathbf{X}(\mathbf{s})^T \hat{\mathbf{Z}}(\mathbf{s}), \quad (9)$$

where

$$\boldsymbol{\beta} = \begin{bmatrix} \boldsymbol{\beta}_1 \\ \vdots \\ \boldsymbol{\beta}_k \end{bmatrix}, \mathbf{X}(\mathbf{s}) = \begin{bmatrix} \mathbf{X}_1(s_1) & \dots & \mathbf{X}_k(s_1) \\ \vdots & \ddots & \vdots \\ \mathbf{X}_1(s_n) & \dots & \mathbf{X}_k(s_n) \end{bmatrix}, \hat{\mathbf{Z}}(\mathbf{s}) = \begin{bmatrix} \hat{Z}(s_1) \\ \vdots \\ \hat{Z}(s_k) \end{bmatrix}$$

New features in WRF-SFIRE and the system in Israel

J. Mandel et al.

Title Page

Abstract

Introduction

Conclusions

References

Tables

Figures

◀

▶

◀

▶

Back

Close

Full Screen / Esc

Printer-friendly Version

Interactive Discussion



We then have the well-known unbiased estimate of the residual variance from the residual sum of squares,,

$$\gamma^2 + \hat{\sigma}^2 = \frac{1}{n-k} \sum_{i=1}^n \hat{\epsilon}(s_i)^2, \hat{\epsilon}(s_i) = \hat{Z}(s_i) - (\mathbf{X}_1(s_i)\boldsymbol{\beta}_1 + \dots + \mathbf{X}_k(s_i)\boldsymbol{\beta}_k). \quad (10)$$

5 The mean and the variance of the estimated field $Z(s)$ are obtained by computing the least squares solution $\boldsymbol{\beta}$ from Eq. (8) and substituting into the trend surface model (Eq. 7), which gives

$$E Z(s) = \mathbf{X}_1(s)\boldsymbol{\beta}_1 + \dots + \mathbf{X}_k(s)\boldsymbol{\beta}_k$$

10 with the mean-squared prediction error

$$\text{Var } Z(s) = \hat{\sigma}^2 + \left(\gamma^2 + \hat{\sigma}^2 \right) \mathbf{x}(s)^T (\mathbf{X}(s)^T \mathbf{X}(s))^{-1} \mathbf{x}(s),$$

where $\mathbf{x}(s) = [\mathbf{X}_1(s), \dots, \mathbf{X}_k(s)]^T$.

15 We use $k = 8$ covariates. The first four covariates are taken to be the current forecast of 10 h fuel moisture, air temperature at 2 m, the surface pressure, and the current rain intensity, which capture the effect of the local state of the atmosphere on the fuel moisture equilibrium. The remaining covariates are the terrain elevations, and three independent functions linear in space, taken as the longitude, the latitude, and a constant.

6 Data management and visualization

20 WRF-SFIRE input is integrated with the standard WRF inputs, prepared by the WRF Preprocessing System (WPS) in WRF. In addition to meteorological data needed for WRF, SFIRE requires high-resolution topography and fuel maps. These are typically available in Geotiff format.

New features in WRF-SFIRE and the system in Israel

J. Mandel et al.

Title Page

Abstract

Introduction

Conclusions

References

Tables

Figures

⏪

⏩

◀

▶

Back

Close

Full Screen / Esc

Printer-friendly Version

Interactive Discussion



New features in WRF-SFIRE and the system in Israel

J. Mandel et al.

Title Page

Abstract

Introduction

Conclusions

References

Tables

Figures

◀

▶

◀

▶

Back

Close

Full Screen / Esc

Printer-friendly Version

Interactive Discussion



Geotiff is a standard for georeferencing metadata in Tagged Image File Format (TIFF) files (Ritter and Ruth, 2000). The Geotiff format is particularly useful for fire related data and fine-scale topography, because it allows a compact representation of data on large meshes with thousand of cells (pixels) in each dimension. Geotiff support has been added to WRF-SFIRE in two forms (Beezley et al., 2011). First, Geogrid files, which can be read by any standard installation of WPS, can be created by a separate utility, which has command line flags to control various Geogrid attributes such as the size of the tiles. The utility creates a header that contains both a description of the tiles and the geocoding (projection and reference points). TopoGrabber (<http://laps.noaa.gov/topograbber>) is a Python application based on this work that is capable of downloading and converting topographical data automatically. Second, the WPS has been modified to read Geotiff files directly. Here, the Geotiff library is wrapped around an abstraction layer that reads the data in tiles. The main advantage is that it can read floating point data directly rather than convert to and from fixed point as required by the Geogrid file format, and it can handle large meshes more easily. Such meshes occur naturally in fire modeling on fine meshes.

WRF output are files in NetCDF format, which need to be input into suitable graphics program. Visualizations paths to various packages are provided, including VAPOR and KML format for Google Maps and Google Earth (Beezley et al., 2012). What has caught the most attention is the utility posted at <https://github.com/jbeezley/wrf2kmz>. This utility converts the NetCDF files from WRF-SFIRE into KML and the compressed variant KMZ, using several Python libraries. This is the software used to generate the Google Maps and Google Earth images in this paper and in our previous work referenced here. It is also behind the prototype web interface (Beezley et al., 2012) as well as the Israel national operational system, described in Sect. 8.

7 Coupling with smoke transport and chemistry

Fire emissions from SFIRE can be input into WRF-Chem (Grell et al., 2005) as chemical species, or into the WRF dynamical core as passive tracers. Chemical species are available only when WRF is built with the CHEM component, while the smoke representation in a form of tracers is available even in the base WRF code. This has a significant advantage, because the full WRF-Chem execution is very computationally intensive, and setting up the model is much more difficult. Both kinds of fire emissions are treated in SFIRE the same way, transparently to the user.

The chemical emissions from a fire are modeled as the mass of the fuel burned times the emission factor for each species, specified in a configuration file as a text table. Files with emission factors from FINN (Wiedinmyer et al., 2011) for the RADM and MOZART chemical models, supported by WRF-Chem, are supplied with the code. The table contains one line for each chemical species, with the amount of per kg of fuel burned for each fuel category. Gas emissions and particulate emissions ($PM_{2.5}$ and PM_{10}) are given in $g\ kg^{-1}$, non-methane organic carbon emissions in $mol\ kg^{-1}$. In every time step, the mass of emission of every species from the fuel burned during the time step is converted to appropriate concentrations in the first layer of cells in WRF, and added to the concentrations of the chemical species advected by the atmosphere and subject to chemical reactions modeled by WRF-Chem.

WRF, with or without Chem, can be run with 8 passive tracers, which are advected by the flow without any chemical reactions. One is a basic tracer, simply advected by the wind field, others have various special properties, such as diffusion. Emission factors for the tracers are specified in the same configuration file as the chemical species, in each fuel category. The emissions are converted by the coupling code to concentrations in the first layer of atmospheric mesh cell, and added to the tracer concentration. Unlike Chem, which is very CPU intensive, turning on the tracers has only a minimal effect on the computational cost. Therefore, modeling emissions transport by the passive tracers is well suited for forecasting in real time.

New features in WRF-SFIRE and the system in Israel

J. Mandel et al.

Title Page

Abstract

Introduction

Conclusions

References

Tables

Figures

◀

▶

◀

▶

Back

Close

Full Screen / Esc

Printer-friendly Version

Interactive Discussion



See the WRF-SFIRE Users Guide OpenWFM (2013) for more details on use, and Kochanski et al. (2013b) for further justification and experimental results. Figure 9 illustrates the simulation of emissions from a large fire.

It is noteworthy that the described coupling includes also integration with aerosol schemes. Depending on the selected options the chemical species emitted from the fire may react in the atmosphere, leading not only to secondary pollutants formations but also to secondary aerosols. The chemical species emitted and formed in the atmosphere, as well as primary and secondary aerosols, may impact radiative and micro-physical process, thus adding new levels of coupling between the fire and the atmosphere.

8 Operational use in Israel

The Israeli national fire forecasting system¹ is built on top of WRF-SFIRE. From the advances described in this paper, the system uses the fire danger maps (Sect. 2), the moisture model (Sect. 4), and the GIS interfaces (Sect. 6).

The system is based on a complete WRF mesoscale weather forecast for Israel (Fig. 10). In order to be able to produce a fire forecast on demand, the weather forecasting system is running from NWS data 4 times daily, with hourly output WRF forecast, from which the fire forecast is made. The WRF forecasts are at 1.333 km resolution (higher than the NWS forecasts), and then they are downscaled further to 444 m. The coupled atmosphere-fire model then runs with 444 m atmospheric mesh resolution and 44.4 m fire mesh resolution. These forecasts can provide high-resolution forecast of not only fires, but severe weather winds/hail, precipitation fields, and terrain-sensitive snow amounts.

¹The Israel national fire forecasting system is an initiative of the Israel Public Security ministry.

New features in WRF-SFIRE and the system in Israel

J. Mandel et al.

Title Page

Abstract

Introduction

Conclusions

References

Tables

Figures

◀

▶

◀

▶

Back

Close

Full Screen / Esc

Printer-friendly Version

Interactive Discussion



New features in WRF-SFIRE and the system in Israel

J. Mandel et al.

Title Page

Abstract

Introduction

Conclusions

References

Tables

Figures

⏪

⏩

◀

▶

Back

Close

Full Screen / Esc

Printer-friendly Version

Interactive Discussion



The fire forecasting system works interactively. When a fire is detected, the user pins the location of the fire by clicking on the interactive map (Fig. 11), or enters the location numerically. The web site then notifies the server system that a WRF-SFIRE forecast has been requested. Given the ignition point, a python script on the server generates a series of namelists with the correct parameters describing the fire simulation domain, which is of the size 36×36 cells on the atmospheric 444 m mesh, and 360×360 cells on the fire 44 m mesh. The ignition point is as close to the center as possible. Static surface data on the fire simulation grid are generated and downscaled data from the 1.333 km simulation are added. The moisture model is run from the operational 1.333 km system's output every 24 h, interpolated to 444 m, and inserted in the fire simulation input for every 1 h simulation interval.

In about 10–12 min, the first hour of the forecast is produced, and within 30 min a six hour fire forecast is staged for download on the website. In addition to animations, the web site also creates Google Earth-based maps of fire spread, intensity, and area coverage. Screen snapshots from the forecast of the 2013 Eshtaol fire in Israel are in Figs. 12 and 13. The forest fire caused the authorities to block Road 38 for three hours, until they controlled the fire intensity by utilizing ground and air support.

The fuel maps are an aggregate of three sources: GIS map of forests from the Jewish National Fund (JNF)'s field operations overlaid by GIS land use map from Israeli national archives. Both are at 61 m resolution. The third source is the USGS 1 km resolution vegetation map, which pads the missing data around the Israeli border and inside the Palestinian authority.

The system also provides a forecast of the fire danger, based on the fireline intensity (Eq. 2) of a potential fire, for the worst-case scenario at which the fire propagates in the direction that results in the highest fire spread rate for the given wind and slope (Sect. 2). This intensity is computed for each cell on the fire simulation grid using the fuel category in the cell, fuel moisture, and local atmospheric conditions. However, to simplify the interface, only values rescaled to the range 0 to 5 at several landmark points are presented to the user (Fig. 14), instead of a map.

Validation of the system currently relies on existing validation studies for WRF-SFIRE (Kochanski et al., 2013c, d). Validation for local conditions, including fuel types, maps, and the effect of the moisture model, is in progress.

The WRF-SFIRE system can provide a valuable and helpful tool to users, and currently it is the only one running operationally. In addition, the weather forecasts themselves are not standard NWS products and put the weather at the scale of the fire attack crews. The system is delivered to subscribers in the firefighting community and other users in Israel to forecast the fire spread and assess the difficulty of suppression and fire danger (Regev et al., 2012).

9 Summary and conclusions

WRF-SFIRE system has significantly evolved since its original description was published in (Mandel et al., 2009, 2011a). The originally simple fire modeling framework advanced by new components that significantly expanded the original capabilities of WRF-SFIRE. The coupling between the atmospheric component of the system and the fuel moisture model allows now for modeling the fire spread, taking into account changes in the fuel properties driven by the weather conditions. In the current form, the model not only creates a weather forecast, but also a fuel moisture forecast, which is used by the fire component of the system to simulate the fire behavior. This new level of interaction embedded into the WRF-SFIRE modeling system has a potential to improve fire behavior representation under conditions when temporal changes in the fuel moisture become important. The model does not assume any diurnal variation in the fuel moisture or intensity. Instead, basic atmospheric properties including temperature, humidity, precipitation, and winds are used for the computation of the fuel moisture and the fire spread at any given time. The fuel moisture component of the system is also used as the core of a fuel moisture data assimilation system, which creates the best estimate of the fuel moisture state, generated, in a gridded from, by a fusion of the observed fuel moisture with the moisture model estimates.

New features in WRF-SFIRE and the system in Israel

J. Mandel et al.

Title Page

Abstract

Introduction

Conclusions

References

Tables

Figures



Back

Close

Full Screen / Esc

Printer-friendly Version

Interactive Discussion



**New features in
WRF-SFIRE and the
system in Israel**J. Mandel et al.

Title Page

Abstract

Introduction

Conclusions

References

Tables

Figures

⏪

⏩

◀

▶

Back

Close

Full Screen / Esc

Printer-friendly Version

Interactive Discussion



The updated version renders also the fire smoke. Depending on the users' requirements, it can be simply treated as a passive tracer advected in the dynamical core of the WRF model, or represented as a mixture of chemically reactive species emitted into the atmosphere, and undergoing chemical and physical reactions. The latter approach, requiring building the model with WRF-Chem, allows not only studying the fire and smoke emission and dispersion, but also investigating the effects of smoke on the atmospheric chemistry. The coupling between the fire model and the chemistry provides a new framework for simulating secondary pollutants created in the atmosphere from the species emitted directly by the fire. Thus, this new functionality allows for rendering the air quality effects of the fire emissions.

The integration with the WRF-Chem is not limited to chemical species. The primary aerosols, and creation of secondary aerosols may be captured with this framework as well. The aerosols emitted by fires may interact with radiation and microphysical processes allowing for another level of coupling between the fire and atmosphere, needed, for example, in order to study processes related to creation of pyrocumulus clouds.

The original ignition mechanism allowing for point and line ignitions has been expanded by the ignitions from an arbitrary fire perimeter. This new functionality allows for continuing the fire spread progression from the observed fire contour, without a need for starting the whole simulation from an initial ignition point or line.

In conclusion, advances in the WRF-SFIRE system include coupling with models of selected other components of the Earth system, which have significant impact on fire behavior (moisture) or are significantly impacted by fire (atmospheric chemistry). Improvements have been directed also towards increasing usability in practice (interfaces with GIS, fire danger assessment, and ignition from perimeter). A new concept of fire-line intensity was also presented. WRF-SFIRE benefits from the integration with WRF, the widespread use of WRF, distribution in the public domain, the general knowledge of operating WRF in the atmospheric science community, and it leverages the standard WRF inputs and outputs.

New features in WRF-SFIRE and the system in Israel

J. Mandel et al.

Title Page

Abstract

Introduction

Conclusions

References

Tables

Figures

◀

▶

◀

▶

Back

Close

Full Screen / Esc

Printer-friendly Version

Interactive Discussion



As a consequence, WRF-SFIRE became one of the first coupled fire-atmosphere models implemented operationally. The newly added capabilities in terms of smoke and fire emission prediction made it an all-in-one model with a potential of generating fire spread, fire emission, plume rise, plume dispersion, and air quality forecast within one integrated framework.

Future work will expand the perimeter ignition approach to the assimilation of fire behavior data, particularly fire location from remote sensing. Addition of the new fire spread models as well as mechanisms for integration with other systems like Blue Sky and CMAQ are also planned.

Acknowledgements. This research was partially supported by the National Science Foundation (NSF) grants AGS-0835579 and DMS-1216481, and National Aeronautics and Space Administration (NASA) grants NNX12AQ85G and NNX13AH9G. This work partially utilized the Janus supercomputer, supported by the NSF grant CNS-0821794, the University of Colorado Boulder, University of Colorado Denver, and National Center for Atmospheric Research. The wildfire system for Israel was funded by the Israel Public Security Ministry.

References

- Balbi, J. H., Morandini, F., Silvani, X., Filippi, J. B., and Rinieri, F.: A physical model for wildland fires, *Combust. Flame*, 156, 2217–2230, doi:10.1016/j.combustflame.2009.07.010, 2009. 1762
- Beezley, J. D., Kochanski, A. K., Kondratenko, V. Y., and Mandel, J.: Integrating high-resolution static data into WRF for real fire simulations, in: Ninth Symposium on Fire and Forest Meteorology, Palm Springs, October 2011, Paper 6.3, available at: <http://ams.confex.com/ams/9FIRE/webprogram/Paper192276.html>, December 2011, 2011. 1773
- Beezley, J. D., Martin, M., Rosen, P., Mandel, J., and Kochanski, A. K.: Data management and analysis with WRF and SFIRE, in: Geoscience and Remote Sensing Symposium (IGARSS) 2012, IEEE, 5274–5277, doi:10.1109/IGARSS.2012.6352419, 2012. 1773
- Byram, G. M.: Combustion of forest fuels, in: *Forest Fire: Control and Use*, edited by: Davis, K. P., McGraw Hill, New York, 61–89, 1959. 1763

New features in WRF-SFIRE and the system in Israel

J. Mandel et al.

Title Page

Abstract

Introduction

Conclusions

References

Tables

Figures

◀

▶

◀

▶

Back

Close

Full Screen / Esc

Printer-friendly Version

Interactive Discussion



- Clark, T. L., Coen, J., and Latham, D.: Description of a coupled atmosphere-fire model, *Int. J. Wildland Fire*, 13, 49–64, doi:10.1071/WF03043, 2004. 1762
- Coen, J. L.: Simulation of the Big Elk Fire using coupled atmosphere-fire modeling, *Int. J. Wildland Fire*, 14, 49–59, doi:10.1071/WF04047, 2005. 1762
- Coen, J., Cameron, M., Michalakes, J., Patton, E., Riggan, P., and Yedinak, K.: WRF-Fire: Coupled weather-wildland fire modeling with the weather research and forecasting model, *J. Appl. Meteorol. Clim.*, 52, 16–38, doi:10.1175/JAMC-D-12-023.1, 2012. 1762
- Fendell, F. E. and Wolff, M. F.: Wind-aided fire spread, in: *Forest Fires, Behavior and Ecological Effects*, edited by: Johnson, E. A. and Miyanishi, K., Academic Press, San Diego, CA, 171–223, 2001. 1762
- Filippi, J. B., Bosseur, F., Pialat, X., Santoni, P., Strada, S., and Mari, C.: Simulation of coupled fire/atmosphere interaction with the MesoNH-ForeFire models, *Journal of Combustion*, 2011, 540390, doi:10.1155/2011/540390, 2011. 1762
- Finney, M. A.: Fire growth using minimum travel time methods, *Can. J. Forest Res.*, 32, 1420–1424, doi:10.1139/x02-068, 2002. 1765
- Finney, M. A.: An overview of FlamMap fire modeling capabilities, in: *Fuels Management – How to Measure Success*, edited by: Andrews, P. L. and Butler, B. W., USDA Forest Service, proceedings RMRS-P-41, 213–220, available at: <http://www.treearch.fs.fed.us/pubs/25948>, 2006. 1763
- Grell, G. A., Peckham, S. E., Schmitz, R., McKeen, S. A., Frost, G., Skamarock, W. C., and Eder, B.: Fully coupled “online” chemistry within the WRF model, *Atmos. Environ.*, 39, 6957–6975, doi:10.1016/j.atmosenv.2005.04.027, 2005. 1774
- Jordanov, G., Beezley, J. D., Dobrinkova, N., Kochanski, A. K., Mandel, J., and Sousedík, B.: Simulation of the 2009 Harmanli fire (Bulgaria), in: *8th International Conference on Large-Scale Scientific Computations*, Sozopol, Bulgaria, 6–10 June 2011, edited by: Lirkov, I., Margenov, S., and Wanśiewski, J., vol. 7116 of *Lecture Notes in Computer Science*, Springer, 291–298, doi:10.1007/978-3-642-29843-1_33, also available as arXiv:1106.4736, 2012. 1762
- Kochanski, A. K., Beezley, J. D., Mandel, J., and Kim, M.: WRF fire simulation coupled with a fuel moisture model and smoke transport by WRF-Chem, in: *13th WRF Users’ Workshop*, 20–24 June 2012, National Center for Atmospheric Research, arXiv:1208.1059, 2012. 1766

New features in WRF-SFIRE and the system in Israel

J. Mandel et al.

Title Page

Abstract

Introduction

Conclusions

References

Tables

Figures

◀

▶

◀

▶

Back

Close

Full Screen / Esc

Printer-friendly Version

Interactive Discussion



Kochanski, A., Jenkins, M. A., Sun, R., Krueger, S., Abedi, S., and Charney, J.: The importance of low-level environmental vertical wind shear to wildfire propagation: proof of concept, *J. Geophys. Res.-Atmos.*, 118, 8238–8252, doi:10.1002/jgrd.50436, 2013a. 1762

Kochanski, A. K., Beezley, J. D., Mandel, J., and Clements, C. B.: Air pollution forecasting by coupled atmosphere-fire model WRF and SFIRE with WRF-Chem, in: Proceedings of 4th Fire Behavior and Fuels Conference, to appear, arXiv:1304.7703, 2013b. 1775

Kochanski, A. K., Jenkins, M. A., Krueger, S. K., Mandel, J., and Beezley, J. D.: Real time simulation of 2007 Santa Ana fires, *Forest Ecol. Manag.*, 15, 136–149, doi:10.1016/j.foreco.2012.12.014, 2013c. 1762, 1766, 1777, 1786

Kochanski, A. K., Jenkins, M. A., Mandel, J., Beezley, J. D., Clements, C. B., and Krueger, S.: Evaluation of WRF-SFIRE performance with field observations from the FireFlux experiment, *Geosci. Model Dev.*, 6, 1109–1126, doi:10.5194/gmd-6-1109-2013, 2013d. 1762, 1777

Kondratenko, V. Y., Beezley, J. D., Kochanski, A. K., and Mandel, J.: Ignition from a Fire Perimeter in a WRF Wildland Fire Model, Paper 9.6, 12th WRF Users' Workshop, 20–24 June 2011, National Center for Atmospheric Research, available at: <http://www.mmm.ucar.edu/wrf/users/workshops/WS2011/WorkshopPapers.php>, retrieved August 2011, 2011. 1765, 1766

Linn, R. R. and Cunningham, P.: Numerical simulations of grass fires using a coupled atmosphere-fire model: basic fire behavior and dependence on wind speed, *J. Geophys. Res.-Atmos.*, 110, D13107, doi:10.1029/2004JD005597, 2005. 1761

Mandel, J., Beezley, J. D., Coen, J. L., and Kim, M.: Data assimilation for wildland fires: ensemble Kalman filters in coupled atmosphere-surface models, *IEEE Contr. Syst. Mag.*, 29, 47–65, doi:10.1109/MCS.2009.932224, 2009. 1761, 1777

Mandel, J., Beezley, J. D., and Kochanski, A. K.: Coupled atmosphere-wildland fire modeling with WRF 3.3 and SFIRE 2011, *Geosci. Model Dev.*, 4, 591–610, doi:10.5194/gmd-4-591-2011, 2011a. 1761, 1762, 1777

Mandel, J., Beezley, J. D., Kochanski, A. K., Kondratenko, V. Y., Zhang, L., Anderson, E., Daniels II, J., Silva, C. T., and Johnson, C. R.: A wildland fire modeling and visualization environment, in: Ninth Symposium on Fire and Forest Meteorology, Palm Springs, October 2011, Paper 6.4, available at: <http://ams.confex.com/ams/9FIRE/webprogram/Paper192277.html>, retrieved December 2011, 2011b. 1764

Mandel, J., Beezley, J. D., Kochanski, A. K., Kondratenko, V. Y., and Kim, M.: Assimilation of perimeter data and coupling with fuel moisture in a wildland fire – atmo-

NHESSD

2, 1759–1797, 2014

New features in WRF-SFIRE and the system in Israel

J. Mandel et al.

Title Page

Abstract Introduction

Conclusions References

Tables Figures

◀ ▶

◀ ▶

Back Close

Full Screen / Esc

Printer-friendly Version

Interactive Discussion



sphere DDDAS, Proceedings of ICCS 2012, Procedia Computer Science, 9, 1100–1109, doi:10.1016/j.procs.2012.04.119, 2012. 1765, 1766

Mell, W., Jenkins, M. A., Gould, J., and Cheney, P.: A physics-based approach to modelling grassland fires, *Int. J. Wildland Fire*, 16, 1–22, doi:10.1071/WF06002, 2007. 1761

OpenWFM: Fire code in WRF release, Open Wildland Fire Modeling e-Community, available at: http://www.openwfm.org/wiki/Fire_code_in_WRF_release, 2012. Accessed November 2013. 1762

OpenWFM: Coupled WRF and SFIRE Model User’s Guide, Open Wildland Fire Modeling e-Community, available at: http://www.openwfm.org/wiki/Users_guide, last access: September 2013, 2013. 1762, 1775

Peace, M., Mattner, T., and Mills, G.: The Kangaroo Island bushfires of 2007: a meteorological case study and WRF-fire simulation, in: Ninth Symposium on Fire and Forest Meteorology, Palm Springs, October 2011, Paper 3.3, available at: <http://ams.confex.com/ams/9FIRE/webprogram/Paper192200.html>, 2011. Accessed November 2013. 1762

Regev, B., Amram, S., and Amit, A.: Six hours ahead – predicting wildfires in real time, *Innovation Exchange*, 16, 34–37, available at: <http://mops.gov.il/English/HomelandSecurityENG/NFservices/Pages/FirePredictionSystem.aspx>, retrieved September 2013, 2012. 1777

Ritter, N. and Ruth, M.: GeoTIFF Format Specification: GeoTIFF Revision 1.0, available at: <http://www.remotesensing.org/geotiff/spec/geotiffhome.html>, retrieved September 2013, 2000. 1773

Rothermel, R. C.: A Mathematical Model for Predicting Fire Spread in Wildland Fires, USDA Forest Service Research Paper INT-115, available at: <http://www.treesearch.fs.fed.us/pubs/32533>, 1972. 1762

Schabenberger, O. and Gotway, C. A.: *Statistical Methods for Spatial Data Analysis*, Chapman & Hall/CRC Texts in Statistical Science, Chapman and Hall/CRC, Boca Raton, FL, 2005. 1771

Sethian, J. A.: *Level set methods and fast marching methods*, in: *Cambridge Monographs on Applied and Computational Mathematics*, vol. 3, 2nd edn., Cambridge University Press, Cambridge, 1999. 1765

Simpson, C. C., Sharples, J. J., Evans, J. P., and McCabe, M. F.: Large eddy simulation of atypical wildland fire spread on leeward slopes, *Int. J. Wildland Fire*, 22, 599–614, doi:10.1071/WF12072, 2013. 1762

- Skamarock, W. C., Klemp, J. B., Dudhia, J., Gill, D. O., Barker, D. M., Duda, M. G., Huang, X.-Y., Wang, W., and Powers, J. G.: A Description of the Advanced Research WRF Version 3, NCAR Technical Note 475, available at: http://www.mmm.ucar.edu/wrf/users/docs/arw_v3.pdf, retrieved December 2011, 2008. 1761
- 5 Van Wagner, C. E. and Pickett, T. L.: Equations and FORTRAN Program for the Canadian Forest Fire Weather Index System, Forestry Technical Report 33, Canadian Forestry Service, 1985. 1766, 1767, 1789
- 640 Vejmelka, M., Kochanski, A. K., and Mandel, J.: Data assimilation of fuel moisture in WRF-SFIRE, in: Proceedings of 4th Fire Behavior and Fuels Conference, to appear, arXiv:1309.0159, 2013. 1770, 1771
- Wiedinmyer, C., Akagi, S. K., Yokelson, R. J., Emmons, L. K., Al-Saadi, J. A., Orlando, J. J., and Soja, A. J.: The Fire INventory from NCAR (FINN): a high resolution global model to estimate the emissions from open burning, *Geosci. Model Dev.*, 4, 625–641, doi:10.5194/gmd-4-625-2011, 2011. 1774

NHESSD

2, 1759–1797, 2014

New features in WRF-SFIRE and the system in Israel

J. Mandel et al.

Title Page

Abstract

Introduction

Conclusions

References

Tables

Figures

◀

▶

◀

▶

Back

Close

Full Screen / Esc

Printer-friendly Version

Interactive Discussion



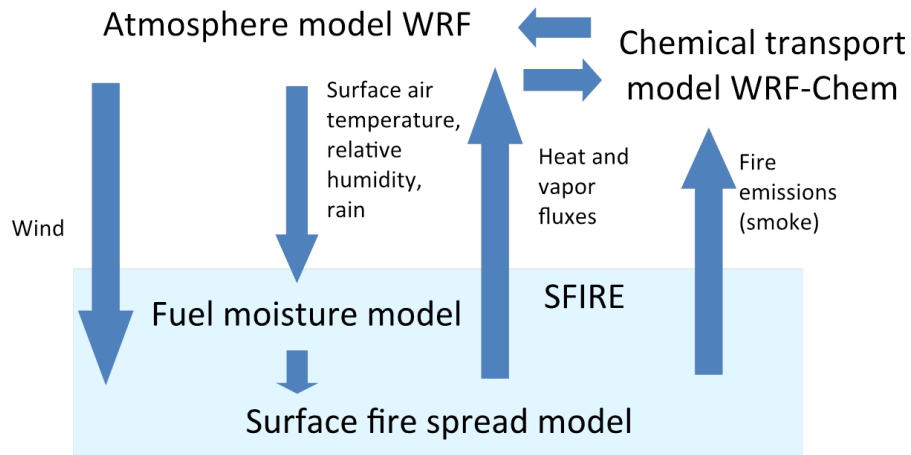


Fig. 1. The overall scheme of WRF-SFIRE.

New features in WRF-SFIRE and the system in Israel

J. Mandel et al.

Title Page

Abstract Introduction

Conclusions References

Tables Figures

◀ ▶

◀ ▶

Back Close

Full Screen / Esc

Printer-friendly Version

Interactive Discussion



New features in WRF-SFIRE and the system in Israel

J. Mandel et al.

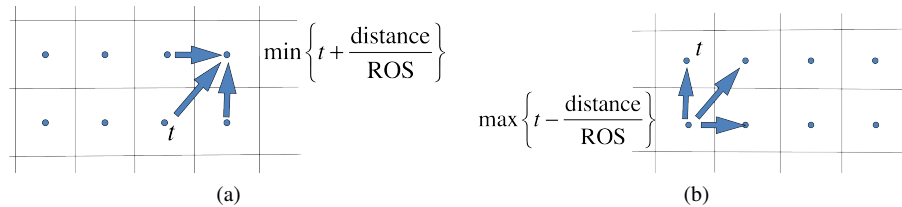


Fig. 2. (a) Propagation of ignition time t to a node from neighboring nodes already on fire. (b) Backtracking (propagation back in time) of ignition time to a node from neighboring nodes where the fire arrived later.

Title Page	
Abstract	Introduction
Conclusions	References
Tables	Figures
◀	▶
◀	▶
Back	Close
Full Screen / Esc	
Printer-friendly Version	
Interactive Discussion	



New features in WRF-SFIRE and the system in Israel

J. Mandel et al.

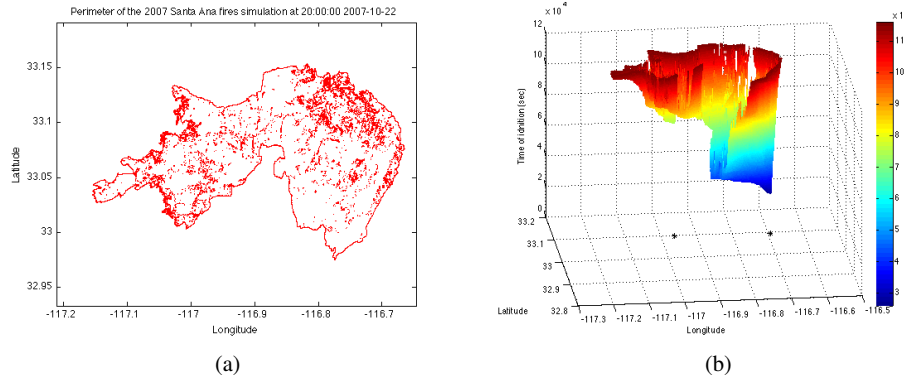


Fig. 3. **(a)** Perimeter of the 2007 Santa Ana fires simulation at 22 October 2007 20:00 UTC Kochanski et al. (2013c). **(b)** Artificial ignition time found by fire propagation back in time from the fire perimeter in **(a)**. The fire consisted of two fires, Witch and Guejito, which started at 21 October 2007 19:15 UTC and 22 October 2007 08:00 UTC, respectively, and subsequently merged. The two peaks on the bottom are the two ignition locations and times, found automatically from the perimeter. The real ignition locations are marked on the bottom of the plot for comparison.

Title Page

Abstract

Introduction

Conclusions

References

Tables

Figures

◀

▶

◀

▶

Back

Close

Full Screen / Esc

Printer-friendly Version

Interactive Discussion



New features in WRF-SFIRE and the system in Israel

J. Mandel et al.

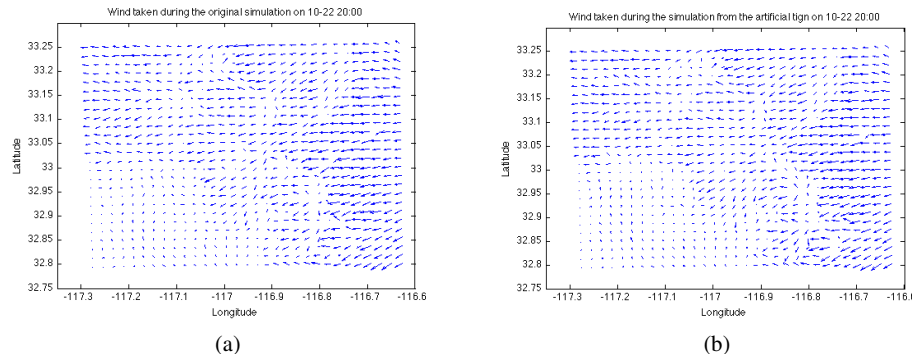


Fig. 4. (a) Horizontal wind at 6.1 m in the 2007 Santa Ana fires simulation at 20:00:00 22 October 2007 UTC. (b) The same wind as in (a), but with the artificial ignition time history from Fig. 3b until 20:00:00 October 2007 UTC. The simulation with artificial fire history, i.e., a spin-up, is not using any data prior to 20:00:00 October 2007 UTC, yet the wind field developed quite close.

Title Page

Abstract

Introduction

Conclusions

References

Tables

Figures

◀

▶

◀

▶

Back

Close

Full Screen / Esc

Printer-friendly Version

Interactive Discussion



New features in WRF-SFIRE and the system in Israel

J. Mandel et al.

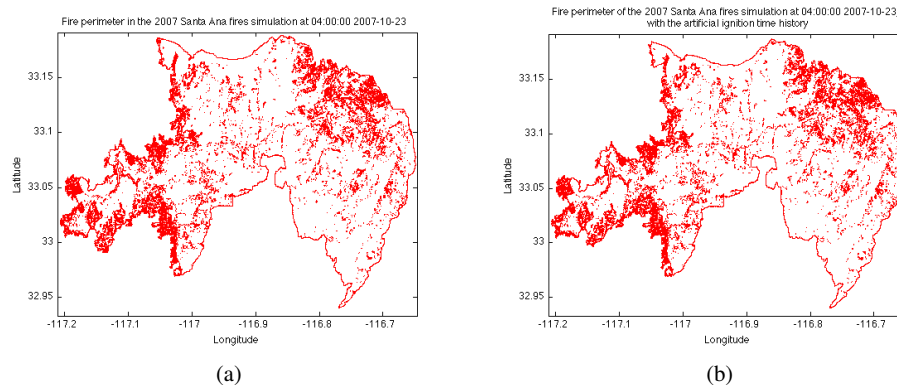


Fig. 5. (a) Fire perimeter in the 2007 Santa Ana fires simulation at 04:00:00 23 October 2007 UTC. (b) The same perimeter as in (a), but with the artificial ignition time history from simulation data (Fig. 3b) at 20:00:00 22 October 2007 UTC. The simulation with artificial fire history, i.e., a spin-up, is not using any data prior to 20:00:00 22 October 2007 UTC, yet the differences in the simulation 6 h later are only minor – compare, e.g., the protuberation at the north-east part of the perimeter.

[Title Page](#)
[Abstract](#)
[Introduction](#)
[Conclusions](#)
[References](#)
[Tables](#)
[Figures](#)
[⏪](#)
[⏩](#)
[◀](#)
[▶](#)
[Back](#)
[Close](#)
[Full Screen / Esc](#)
[Printer-friendly Version](#)
[Interactive Discussion](#)


New features in WRF-SFIRE and the system in Israel

J. Mandel et al.

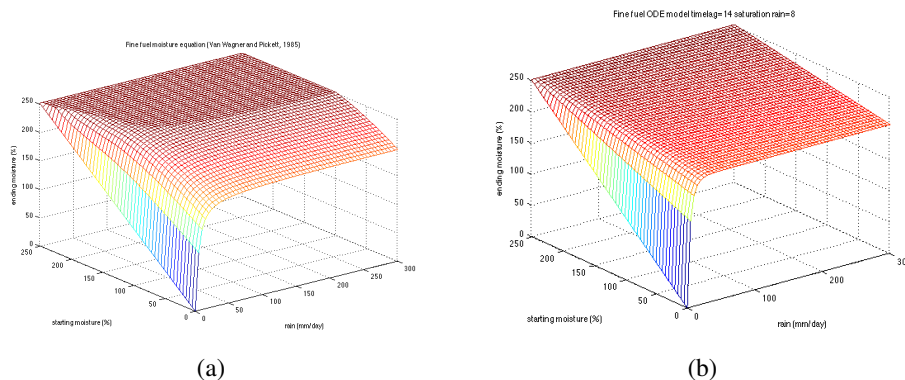


Fig. 6. Response of fine fuels to rain over 24 h **(a)** following Van Wagner and Pickett (1985) **(b)** from the time-lag model (Eq. 4) by a calibration of coefficients.

Title Page

Abstract

Introduction

Conclusions

References

Tables

Figures

◀

▶

◀

▶

Back

Close

Full Screen / Esc

Printer-friendly Version

Interactive Discussion



New features in WRF-SFIRE and the system in Israel

J. Mandel et al.

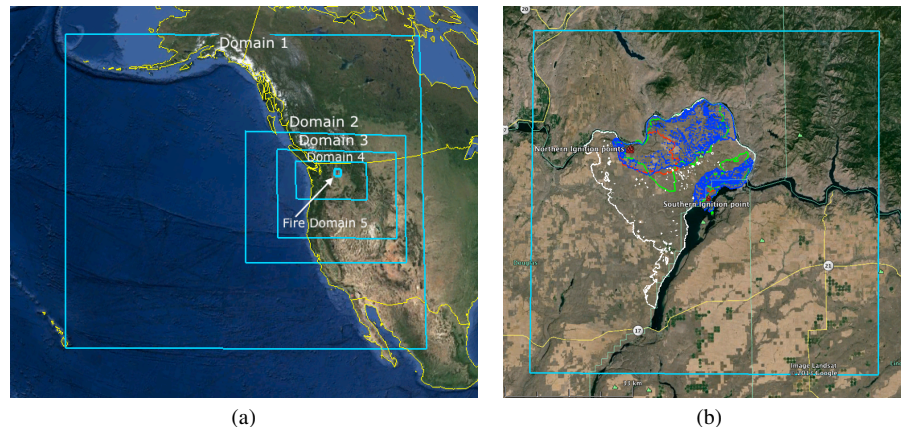


Fig. 7. (a) WRF-Sfire multidomain setup used for the simulation of the 2012 Barker Complex fire (WA). (b) Comparison between the fire perimeters simulated with the constant fuel moisture of 11.6 % (red contour), 6.38 % (white contour), and with the variable fuel moisture simulated by the fuel moisture model (blue contour). The remotely sensed fire perimeter detected on 13 September 2012 07:44 UTC is shown as the green contour.

[Title Page](#)[Abstract](#)[Introduction](#)[Conclusions](#)[References](#)[Tables](#)[Figures](#)[◀](#)[▶](#)[◀](#)[▶](#)[Back](#)[Close](#)[Full Screen / Esc](#)[Printer-friendly Version](#)[Interactive Discussion](#)

New features in WRF-SFIRE and the system in Israel

J. Mandel et al.

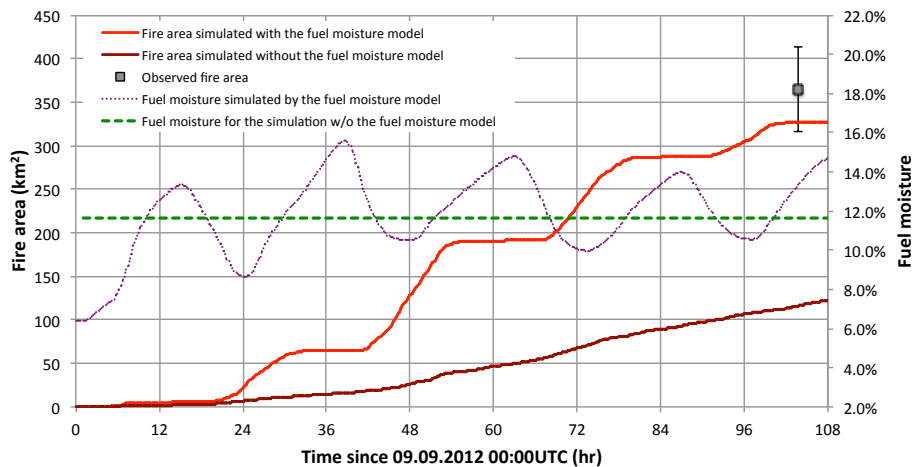


Fig. 8. Time series of the WRF-Sfired simulated fire area (solid lines), and the fuel moisture (dashed lines). The grey point shows the fire area observed on 13 September 2012 07:44 UTC. The error bar shown on the picture is estimated from the spread of different reported perimeters.

Title Page

Abstract

Introduction

Conclusions

References

Tables

Figures

◀

▶

◀

▶

Back

Close

Full Screen / Esc

Printer-friendly Version

Interactive Discussion



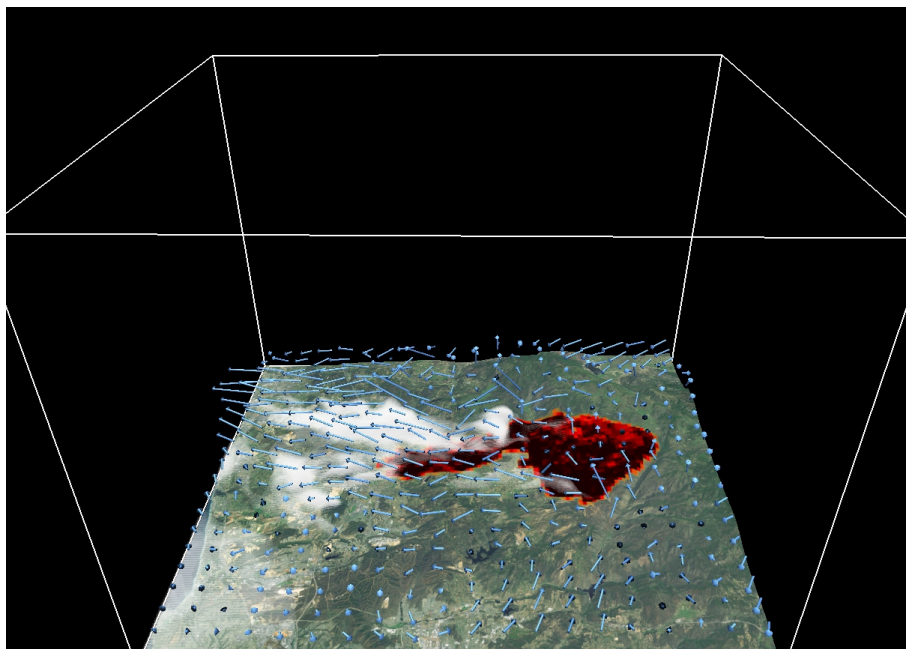


Fig. 9. Illustration of smoke transport and dispersion from a simulation of 2007 Santa Ana fires by WRF-SFIRE coupled with WRF-Chem. Shown are the boundary layer circulation in the plume and PM_{25} concentration.

New features in WRF-SFIRE and the system in Israel

J. Mandel et al.

Title Page

Abstract

Introduction

Conclusions

References

Tables

Figures

⏪

⏩

◀

▶

Back

Close

Full Screen / Esc

Printer-friendly Version

Interactive Discussion



New features in WRF-SFIRE and the system in Israel

J. Mandel et al.



Fig. 10. Weather forecast for Israel, which serves as a basis for the fire forecast. Wind and temperature shown to the user.

Title Page

Abstract Introduction

Conclusions References

Tables Figures

◀ ▶

◀ ▶

Back Close

Full Screen / Esc

Printer-friendly Version

Interactive Discussion



NHESSD

2, 1759–1797, 2014

New features in WRF-SFIRE and the system in Israel

J. Mandel et al.



Fig. 11. Interactive fire ignition.

Title Page

[Abstract](#) [Introduction](#)
[Conclusions](#) [References](#)
[Tables](#) [Figures](#)

⏪ ⏩
◀ ▶

[Back](#) [Close](#)

[Full Screen / Esc](#)

[Printer-friendly Version](#)

[Interactive Discussion](#)



NHESSD

2, 1759–1797, 2014

New features in WRF-SFIRE and the system in Israel

J. Mandel et al.

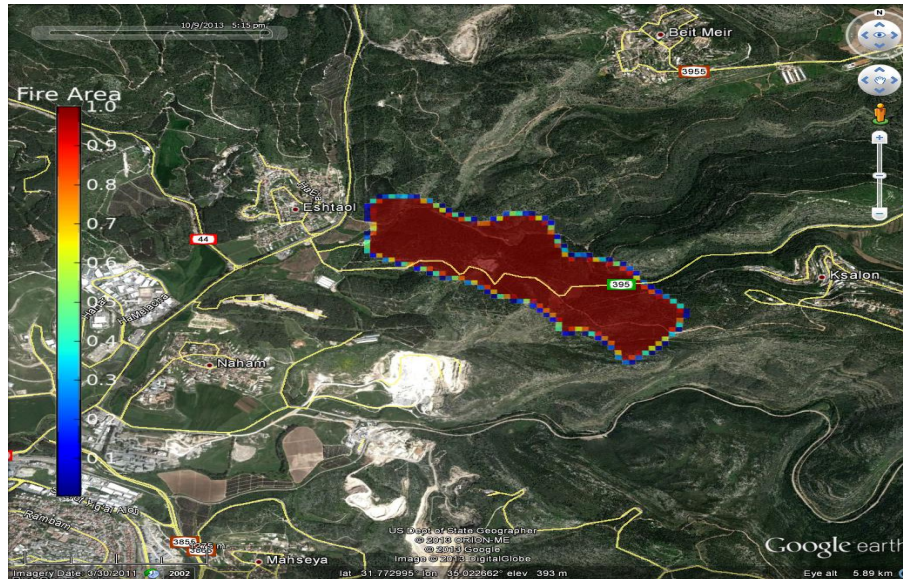


Fig. 12. Fire area and fireline forecast for the fire area of a real fire that was ignited at 11:15 LT 9 October 2013. Fire area value of 1.0 means that the whole grid cell is burning.

Title Page

Abstract

Introduction

Conclusions

References

Tables

Figures

◀

▶

◀

▶

Back

Close

Full Screen / Esc

Printer-friendly Version

Interactive Discussion



New features in WRF-SFIRE and the system in Israel

J. Mandel et al.

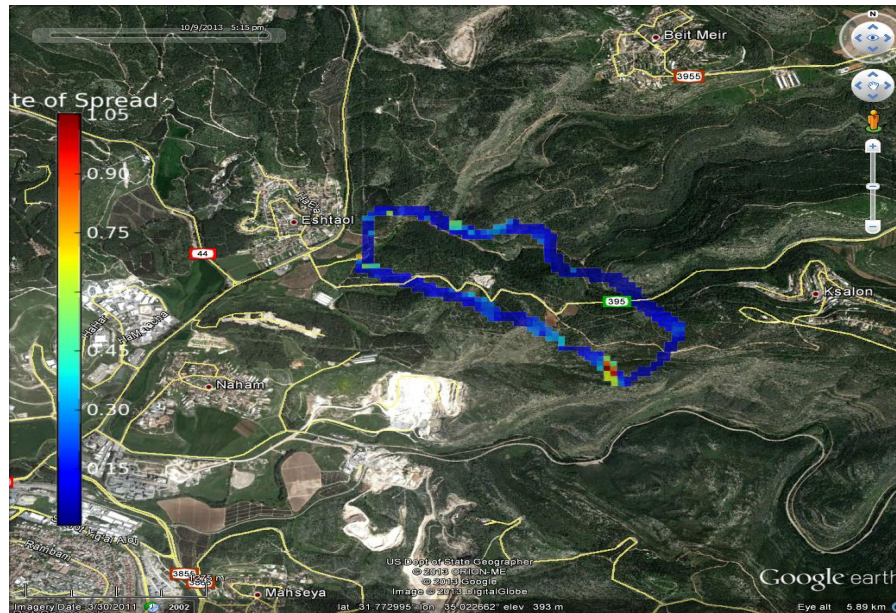


Fig. 13. Forecast of fire rate of spread in the vicinity of the fireline of the fire from Fig. 12.

Title Page

Abstract

Introduction

Conclusions

References

Tables

Figures

⏪

⏩

◀

▶

Back

Close

Full Screen / Esc

Printer-friendly Version

Interactive Discussion



New features in WRF-SFIRE and the system in Israel

J. Mandel et al.



Fig. 14. Fire danger forecast, based on the fireline intensity of a potential fire propagating in the direction with the maximum rate of spread.

Title Page

Abstract Introduction

Conclusions References

Tables Figures

◀ ▶

◀ ▶

Back Close

Full Screen / Esc

Printer-friendly Version

Interactive Discussion

